



Universiteit  
Leiden  
The Netherlands

## **Non-invasive assessment of human brown adipose tissue: development of robust imaging methods to facilitate clinical translation**

Sardjoe Mishre, A.S.D.

### **Citation**

Sardjoe Mishre, A. S. D. (2023, September 5). *Non-invasive assessment of human brown adipose tissue: development of robust imaging methods to facilitate clinical translation*. Retrieved from <https://hdl.handle.net/1887/3638467>

Version: Publisher's Version

License: [Licence agreement concerning inclusion of doctoral thesis in the Institutional Repository of the University of Leiden](#)

Downloaded from: <https://hdl.handle.net/1887/3638467>

**Note:** To cite this publication please use the final published version (if applicable).



# Chapter 5

Image registration and mutual thresholding enable low inter-image variability across dynamic MRI measurements of supraclavicular brown adipose tissue during mild-cold exposure

This chapter has been submitted for publication.

Aashley S.D. Sardjoe Mishre  
Borja Martinez-Tellez  
Maaike E. Straat  
Mariëtte R. Boon  
Oleh Dzyubachyk  
Andrew G. Webb  
Patrick C.N. Rensen  
Hermien E. Kan

## ABSTRACT

Activated brown adipose tissue (BAT) enhances lipid catabolism, and improves cardio-metabolic health. Quantitative MRI of the fat fraction (FF) of supraclavicular BAT (scBAT) is a promising non-invasive measure to assess BAT activity, but suffers from high scan variability. We aimed to test the effects of co-registration and mutual thresholding on the scan variability in a fast (one-minute) time-resolution MRI protocol for assessing scBAT FF changes during cold exposure. Ten volunteers (age:  $24.8 \pm 3.0$  years; BMI:  $21.2 \pm 2.1$  kg/m<sup>2</sup>) were scanned during thermoneutrality (32°C; 10 min) and mild-cold exposure (18°C; 60 min) using a 12-point gradient-echo sequence (70 consecutive scans with breath-holds, 1.03 min per dynamic).

Dynamics were co-registered to the first thermoneutral scan, which enabled drawing of single regions of interest (ROIs) in the scBAT depot, and the trapezius muscle and humerus bone as control tissues. Voxel-wise FF changes were calculated at each time point and averaged across ROIs. We applied mutual FF thresholding, where voxels were included if their FF was >30% (scBAT), >0% (muscle) and >70% (bone) in the reference scan and the registered dynamic. The efficacy of the co-registration was determined by using a moving average, and comparing the mean squared error (MSE) of residuals between registered- and non-registered data. Registered scBAT  $\Delta$ FF was compared to single-scan thresholding using the moving average method. scBAT FF changes were compared to control tissues using a mixed model analysis. Registered scBAT  $\Delta$ FF had lower MSE values than non-registered data ( $0.07\% \pm 0.05\%$  versus  $0.16\% \pm 0.14$ ;  $p < 0.05$ ), and mutual thresholding reduced the scBAT  $\Delta$ FF variability by 30%. Relative to the control tissues, scBAT FF decreased during the last 30 minutes of cooling by  $0.71 \pm 0.83\%$  and  $0.74 \pm 0.84\%$  in muscle and bone, respectively.

We demonstrate that co-registration and mutual thresholding improve stability of the data two-fold, enabling assessment of small changes in FF upon cold exposure.

## 5.1 INTRODUCTION

Brown adipose tissue (BAT) is a thermogenic tissue that combusts fatty acids and glucose into heat. The most potent activator of BAT is cold exposure, upon which norepinephrine (NE) is released by sympathetic nerve endings in BAT: NE binds to  $\beta$ -adrenergic receptors on the brown adipocytes and activates a thermogenic program, including intracellular lipolysis<sup>1</sup>. Chemical energy is converted to heat via the BAT-specific uncoupling protein 1 (UCP-1), and BAT activation leads to the combustion of intracellular lipid stores. These lipid stores are subsequently replenished by extracting lipids and glucose from the blood<sup>2</sup>. Since BAT is involved in lipid- and glucose metabolism, many studies have addressed its protective role against obesity and cardiometabolic diseases<sup>3-6</sup>. In addition to using cold exposure<sup>7</sup>, pharmacological compounds such as mirabegron can also activate BAT<sup>8</sup>.

BAT activity during such challenges is usually indirectly assessed by quantifying the glucose uptake of the radioactively labelled glucose analogue [<sup>18</sup>F]fluorodeoxyglucose, using positron emission tomography/computed tomography (PET-CT)<sup>9</sup>. However, PET-CT suffers from well-recognized limitations: the invasive nature and radiation dose increase the participation burden and hamper longitudinal studies. In addition, this modality visualizes the glucose uptake, while BAT predominantly combusts lipids rather than glucose<sup>10</sup>. Most importantly, glucose uptake by BAT is reduced in individuals who are insulin resistant such as in obesity and type 2 diabetes, and therefore the technique is much less reliable in these patients<sup>10</sup>.

Magnetic resonance imaging (MRI) is a non-invasive and safe method for estimating supraclavicular BAT (scBAT) activity during cold exposure using chemical-shift-based water-fat separation sequences such as the Dixon technique for quantitative fat fraction (FF) mapping<sup>11</sup>. In previous studies, cold-induced supraclavicular FF changes between -0.4 and -3.5% have been reported<sup>11,12</sup>. Most of these studies have either used pre- and post-cooling assessments of scBAT FF<sup>12</sup> or have been performed without the use of image registration<sup>13-15</sup> or breath-holds<sup>16-18</sup>. This may have resulted in increased variability in estimated FF changes over time since scBAT is located in the supraclavicular area, which renders measurements prone to movement artifacts. In addition, most studies acquired images at a relative coarse time resolution of 2.5-5 minutes<sup>13,18,19</sup>. Since BAT activation occurs within 10 minutes after applying a cold stimulus<sup>13,20</sup>, this temporal resolution may not be sufficient to study the short-time dynamics of BAT in detail.

Here, we aimed to minimize inter-scan variability by applying breath-holds and non-rigid image registration in a MRI protocol with a high temporal resolution for assessing FF dynamics in scBAT during cold exposure.

## 5.2 MATERIALS AND METHODS

### 5.2.1 Subjects

Ten healthy volunteers with an age between 18 and 25 years and a body mass index (BMI) between 18 and 25 kg/m<sup>2</sup> were recruited from our local healthy volunteer database and by using flyers. Exclusion criteria were the use of any medication known to affect lipid and/or glucose metabolism, recent excessive weight change, smoking and contra-indications for MRI. The study was performed in accordance with the Declaration of Helsinki and approved by the local medical ethics committee. Written consent was obtained from all participants prior to participation.

### 5.2.2. Study design and cooling protocol

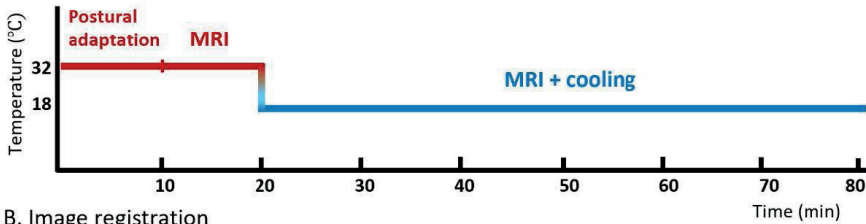
Participants were instructed to fast overnight for 12 hours, and to withhold from alcohol and caffeine consumption for 24 hours prior to the experiment. On the day of the experiment, participants were asked to wear a t-shirt, shorts and slippers. Body weight and height were measured and BMI was calculated by dividing the body weight by height squared (kg/m<sup>2</sup>). Participants then entered the MRI suite and were positioned on the MR table. A water circulating blanket, Blanketrol® III hyper-hypothermia system (Cincinnati Sub-Zero, Cincinnati, OH, USA), was placed on top of the participant and the temperature was initially set to 32°C. After 10 minutes at thermoneutrality, data were acquired for 10 minutes before the temperature was lowered to 18°C to initiate the standardized cooling protocol for BAT activation (**Fig. 1**). Every 10 to 15 minutes, participants were asked to score their cold perception using a numeric rating scale (NRS; 1=comfortable and 10=extremely cold). The total cooling duration was 60 minutes. The experiment was stopped in case of self-reported shivering. Scans were conducted at the same time of day in all participants (10.30 AM-12.00 PM) between April 16<sup>th</sup> and July 23<sup>rd</sup>, 2021.

### 5.2.3. Image acquisition

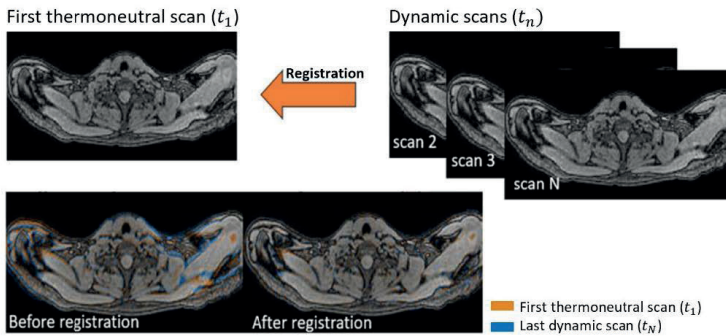
Data were acquired on a 3T MRI scanner (Philips Ingenia Elition X, Philips Healthcare, Best, The Netherlands) using a 16-channel head-and-neck coil, a 12-channel phased array placed on top of the subject, as well as the in-table 16-channel array for signal reception. A three-dimensional multi-gradient-echo sequence with twelve echoes (mDIXON Quant) was used with the following parameters: repetition time TR = 12 ms, first echo time TE = 1.12 ms, echo time separation  $\Delta TE = 0.87$  ms, flip angle = 3°, field-of-view of 400×229×134 mm<sup>3</sup> (Right-Left, Foot-Head, Anterior-Posterior), 2.1 mm isotropic resolution and breath hold time of 16 s. We used twelve echoes to ensure reliable T2\* decay estimation<sup>21</sup>. The acquisition time per scan was 1.03 minutes, which yielded in total 70 scans: 10 scans at thermoneutrality and 60 scans during cooling.

To evaluate the stability of the sequence over time, a commercial phantom that consisted of twelve water-fat emulsion tubes (Calimatrix<sup>21</sup>) with low FFs (0%, 2.7%, 5.3%, 7.8%), intermediate FFs (10.1%, 15.5%, 20.4%, 23.6%) and high FFs (30.2%, 39.9%, 50.1%, 100%) was scanned for one hour at room temperature using a 16-channel head-and-neck coil with the previously described parameter settings.

#### A. MRI and cooling protocol



#### B. Image registration



#### C. ROI delineation and FF thresholding

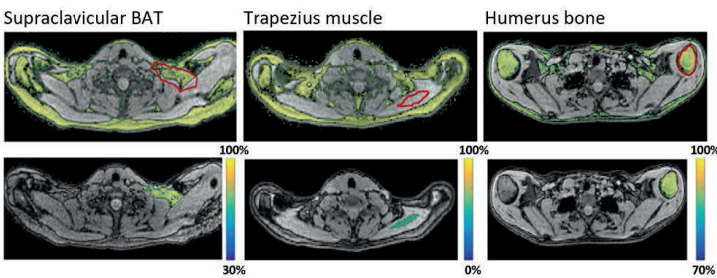


**Figure 1.** A) Participants underwent a standardized cooling protocol to activate BAT. After 20 minutes at thermoneutrality (32°C), the temperature was set to 18°C for one hour. Images were acquired during the last 10 minutes at thermoneutrality and during cooling. B) The first thermoneutral scan was used as a reference image, and all subsequent dynamic scans were co-registered to the first scan. First echo magnitude images were used for co-registration and the resulting transformation matrix was used to deform the FF map of each dynamic to match the image coordinates of the first thermoneutral scan. C) ROIs were only drawn on the first thermoneutral scan and voxels below 30% FF were mutually excluded in both fixed and dynamic scans to avoid inclusion of non-fatty tissue for scBAT. No FF thresholds were used for muscle and a 70-100% mutual FF threshold range was used for the humerus bone. Fat fraction (FF), Region of interest (ROI).

## 5.2.4 Water-fat data reconstruction

An in-house developed complex-based fitting algorithm was used to estimate voxel-based water and fat signals based on the known frequencies and amplitudes of the multiphase lipid spectrum<sup>22</sup> and a mono-exponential decay of  $T2^*$ <sup>23</sup>. The field inhomogeneity map obtained from the mDIXON Quant sequence was used as an initial estimate in the water-fat separation model. FF maps were subsequently calculated by dividing the fat signal by the sum of the water and fat signals in each voxel across the three-dimensional image.

## 5.2.5 Phantom data analysis

For analysis of the phantom data, a region of interest (ROI) was manually delineated for each phantom tube on the first scan. A single rectangular ROI was placed in the middle of each tube and ROIs were directly transferred to all subsequent dynamic scans. For each tube, voxel-wise FF differences between the first scan and each dynamic scan  $i$ ,  $\Delta FF_i(x,y,z) = FF_i(x,y,z) - FF_1(x,y,z)$ , were computed and averaged across the ROI.

## 5.2.6 In vivo image registration and ROI segmentation

For analysis of the *in vivo* data, first-echo magnitude images of each dynamic were co-registered to the first thermoneutral scan (reference scan) using the open-access registration toolbox Elastix<sup>23</sup> (**Fig. 1B**). Dynamic images were iteratively deformed using a three-dimensional B-spline transform with a  $10 \times 10 \times 10$  mm<sup>3</sup> grid, adaptive stochastic gradient descent with two resolutions, 4000 iterations, and the Mattes mutual information as the similarity metric<sup>24</sup>. As a result, ROIs only needed to be delineated on the first thermoneutral scan. ROIs were coarsely delineated in the scBAT depot, and we applied a mutual FF thresholding approach, where voxels were only included in the analysis, if their FF was above 30% in both the reference scan and the registered dynamic. As a control, ROIs were also drawn in the trapezius muscle and the humeral bone using 0–100% and 70–100% mutual FF threshold levels, respectively. Voxel-wise FF differences between the reference scan and each dynamic scan  $i$ :  $\Delta FF_i(x,y,z) = FF_i(x,y,z) - FF_{TN1}(x,y,z)$  were calculated and averaged across the ROI.

## 5.2.7 Data analysis and statistics

The following analyses were performed to: i) determine the stability of the high-temporal-resolution MRI protocol, ii) evaluate the validity and added value of image registration, iii) evaluate the added value of mutual FF thresholding, and iv) compare cold-induced scBAT FF changes with control tissues.

### *Evaluating the stability of our high-temporal-resolution MRI protocol in the phantom*

The temporal stability of the MRI protocol was evaluated by assessing FF changes of each phantom tube. For each tube, a trendline was fitted of scBAT FF changes using a linear

regression analysis. To quantify any decreasing or increasing trends, the vertical distance between the last and first point along the fitted trend line was determined.

Next, a moving average was computed along the FF changes of each phantom tube using a [-3,3] time window. As a measure of the variability, the mean squared error (MSE) of residuals between the moving average and the measured FF data was calculated. This method will be further referred to as the “*moving average method*”.

#### *Evaluating the validity and added value of co-registration of in vivo data*

The validity of the co-registration was assessed for each subject by registering the first thermoneutral (reference) scan to the dynamics in order to emulate the same extent of motion in the reference scan. This yielded a forward transformation (reference  $\rightarrow$  dynamic) for each dynamic. Each dynamic scan was subsequently registered to the reference scan to obtain the backward transformation matrix (dynamic  $\leftarrow$  reference). For each dynamic, the forward and backward transformations were composed and applied to the reference scan to evaluate the registration error. FF difference maps were generated between the resulting deformed reference scan and the original one. The registration error was consecutively computed for each dynamic by taking the voxel-wise FF differences between the original reference scan and the deformed one,  $\Delta FF_{\text{error}}(x,y,z) = FF_{\text{def}}(x,y,z) - FF_{\text{TN1}}(x,y,z)$ , and averaged across the ROI in the scBAT area. To quantify any decreasing or increasing trends of the registration error, a trendline was fitted along the  $\Delta FF_{\text{error}}$  time series for each participant. As a measure of the variability along the  $\Delta FF_{\text{error}}$  time series, MSE values were computed for each participant using the moving average method.

The added value of the co-registration method was determined by comparing scBAT FF changes during cold exposure between registered- and non-registered data. The moving average method was used to determine the variability of scBAT  $\Delta FF$  obtained from registered and non-registered data for each participant separately, as a measure for the intra-subject variability. Paired t-tests were performed to compare the intra-subject variability between registered and non-registered data.

#### *Evaluating the added value of mutual FF thresholding of in vivo data*

The added value of mutual FF thresholding was assessed by comparing scBAT FF changes obtained from mutual and single FF thresholding using the moving average method. Single FF thresholding was performed by applying a 30-100% FF threshold to each individual dynamic. Data were separately analysed for registered and non-registered scBAT FF changes, and paired t-tests were performed to compare the within-subject variability between mutual- and single FF thresholded data.

### *Comparing the scBAT FF response to control tissues (skeletal muscle and humerus bone)*

Next, it was determined whether the scBAT FF changes over time differed from these estimated in control tissues: the trapezius muscle and the humerus bone. The moving average method was used to determine the variability of FF for both control tissues. Afterwards, the  $\Delta FF$  time series of each control tissues were subtracted from the scBAT  $\Delta FF$  time series, which yielded two difference curves:  $\Delta FF_{scBAT} - \Delta FF_{trapezius}$  and  $\Delta FF_{scBAT} - \Delta FF_{humerus}$ . To prevent an overestimation of the statistical power, FF differences were averaged across every 10 minutes along the measurement interval resulting in seven temporal measurements. For each control tissue, it was determined whether the difference curve deviated from zero using a mixed model analysis. Thermal perception scores were compared between thermoneutrality and each cooling period using the Wilcoxon signed-rank test. Data analysis was performed using Matlab (version R2021a) and SPSS. Results were considered significant at  $p < 0.05$ .

## 5.3 RESULTS

Ten young and lean subjects (age=24.8±3.0 years and BMI=21.2±2.1 kg/m<sup>2</sup>) participated. Nine participants were female and one participant was male. All participants completed the protocol. Participants reported significantly higher cold perceptions compared to thermoneutrality (NRS=1.5±0.7) after 15 minutes of cooling (NRS=3.7±1.0;  $p=0.004$ ), 30 minutes of cooling (NRS=3.6±0.9;  $p=0.005$ ), 45 minutes of cooling (NRS=3.6±1.1;  $p=0.007$ ) and after 1-h of cooling (NRS=4.1±1.3;  $p=0.005$ ).

### 5.3.1 Phantom tubes with low, intermediate and high FFs show stable $\Delta FF$ measurements

Phantom tubes with low, intermediate, and high FFs showed stable  $\Delta FF$  measurements over time (**Fig. 2A-C**). The vertical distance along the fitted trendlines were  $-0.05\% \pm 0.08\%$  for the low FF tubes,  $0.27\% \pm 0.10\%$  for the intermediate FF tubes and  $0.05\% \pm 0.20\%$  for the high FF tubes. The MSE values were  $0.02 \pm 0.005\%$  for the low FF tubes,  $0.02 \pm 0.005\%$  for the intermediate FF tubes and  $0.02 \pm 0.01\%$  for the high FF tubes.

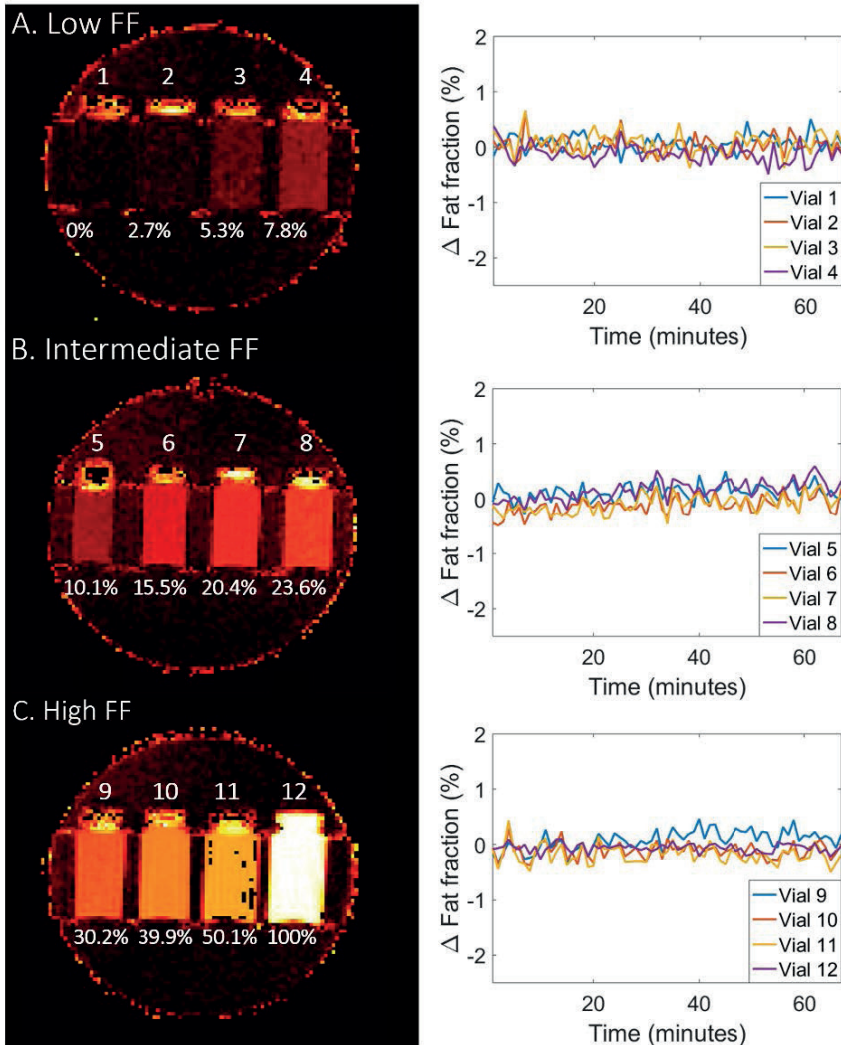


**Figure 2.** Fat fraction changes are plotted as a function of time for water-fat emulsion tubes in the A) low fat fraction (FF) range (0%, 2.7%, 5.3%, 7.8%), B) intermediate FF range (10.1%,15.5%,20.4%,23.6%) and C) high FF range (30.2%,39.9%,50.1%,100%).

### 5.3.2 Co-registration of in vivo data shows a negligible registration error over time and reduces the variability compared to non-registered data

The co-registration error caused substantially small FF changes over time (MSE:0.001%±0.002%; **Fig. 3A**), and resulted in a vertical distance of 0.003±0.01% along the fitted trendlines. The within-subject MSE values of registered scBAT  $\Delta$ FF were lower compared to non-registered data (MSE: 0.07%±0.05% versus MSE:0.16%±0.14% respectively;  $p=0.01$ ; **Fig. 3B-C**), and resulted in an increase in the  $\Delta$ FF response over time by a factor of two.

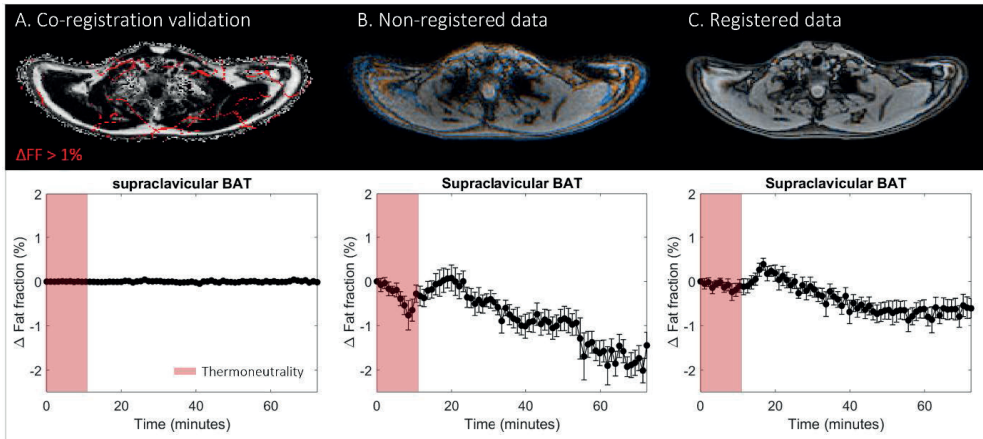


**Figure 3.** Fat fraction changes for the co-registration validation analysis (A), non-registered data (B) and registered data (C). scBAT fat fraction (FF) changes above 1% are shown in red in (A). Image overlap between the first thermo-neutral (reference) scan and the last dynamic are shown for B and C, where the reference scan and the last dynamic are shown in orange and blue, respectively. Red denotes thermonutrality.

### 5.3.3. Mutual FF thresholding reduces the variability of registered scBAT $\Delta$ FF data compared to single FF thresholding, while it increases the variability for non-registered data

For non-registered data, mutual FF thresholding increased the MSE values compared to single FF thresholding ( $0.16\% \pm 0.14\%$  versus  $0.13\% \pm 0.13\%$ ;  $p=0.01$ ; **Fig. 4A**). For registered data, mutual FF thresholding reduced the MSE values compared to single FF thresholding, but this was not significant (MSE:  $0.07\% \pm 0.05\%$  versus MSE:  $0.10\% \pm 0.10\%$ ;  $p=0.1$ ; **Fig. 4B**).

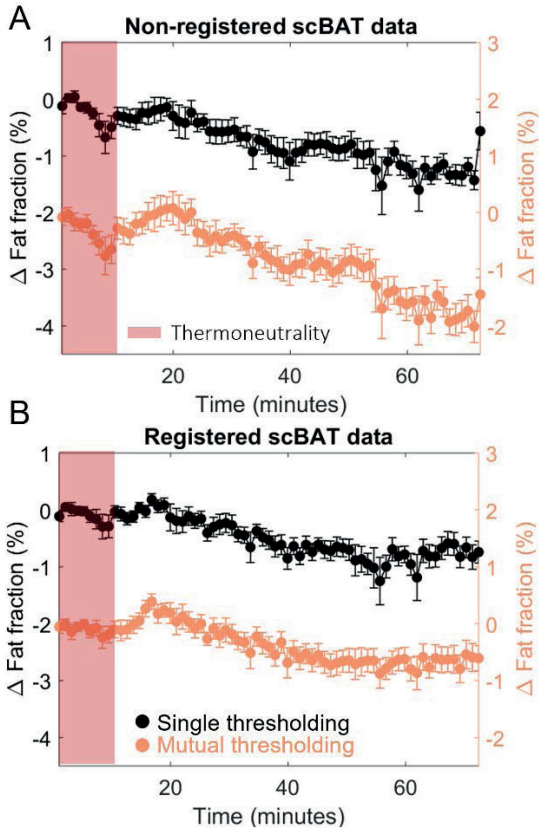


**Figure 4.** Fat fraction changes are shown for non-registered data (A) and registered data (B) after applying a 30-100% single fat fraction (FF) threshold (black) and mutual FF threshold (orange). Red denotes thermoneutrality.

### 5.3.4 The FF response in scBAT differs from control tissues during the last 30 minutes of cooling

As expected, FF changes in the trapezius muscle and the humerus bone revealed no specific FF patterns during cooling with small changes over time (skeletal muscle MSE:  $0.05 \pm 0.05\%$  and humerus bone MSE:  $0.11 \pm 0.06\%$ ; **Fig. 5A-B**).  $\Delta$ FF in scBAT was significantly reduced by  $-0.68 \pm 0.76\%$ ,  $-0.80 \pm 0.88\%$  and  $-0.66 \pm 0.81\%$  compared to  $\Delta$ FF in the trapezius muscle at time intervals 5 (40-50 minutes), 6 (50-60 minutes) and 7 (60-70 minutes), respectively. Compared to the humerus bone, scBAT  $\Delta$ FF was significantly reduced by  $-0.39 \pm 0.61\%$  and  $-0.43 \pm 0.46\%$  at time intervals 5 and 6 (**Fig. 5C**).

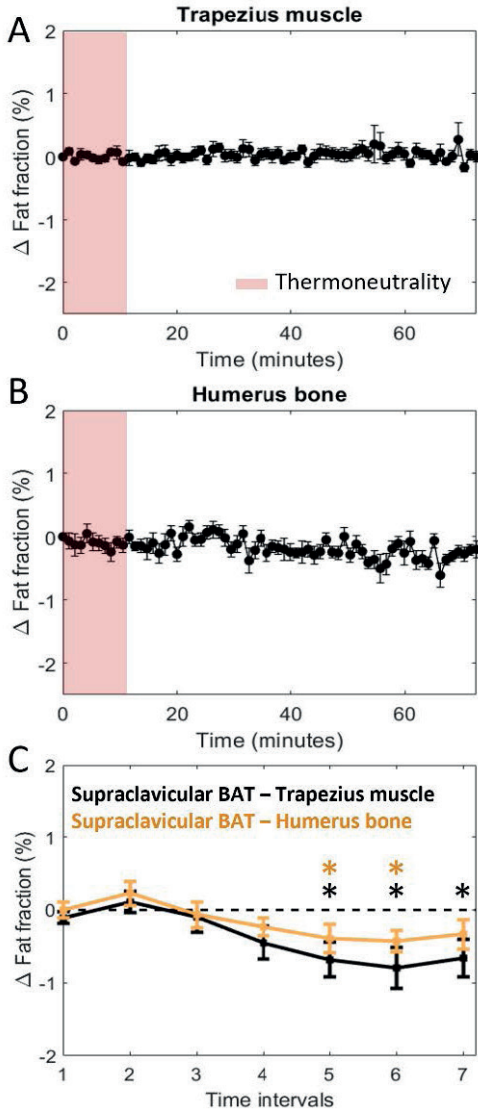


**Figure 5.** Fat fraction changes for the trapezius muscle and humerus bone are shown in A and B. Fat fraction (FF) difference curves between supraclavicular BAT, the trapezius muscle (black) and the humerus bone (orange) are shown in C. The FF difference curves are averaged across every 10 minutes along the measurement, which yielded seven time intervals. \* $P < 0.05$ .

## 5.4 DISCUSSION

In this work, we developed a 1-minute time resolution protocol for the assessment of sc-BAT FF changes using breath-holds and co-registration to minimize motion-induced variation. Our MRI protocol showed a high stability of FF in the phantom, and co-registration and mutual FF thresholding of *in vivo* data improved the stability of scBAT FF changes compared to non-registered data. Upon cold exposure, FF first increased in scBAT, and then decreased compared to control tissues.

Our MRI protocol resulted in a low variability of less than 0.1% FF in all phantom tubes over the entire scan duration of 70 minutes. No FF trend of 0.5% or higher occurred in any of the phantom tubes. In previous work, similar results were found regarding the repeatability of FF measurements in the Calimetrix phantom<sup>21</sup>, where a FF difference of 0.8% or lower between measurements that were performed on three different occasions was shown. Our data additionally show that the stability across FF measurements is maintained while acquiring images consecutively for 1-hour using a 1-minute time resolution. As such, influences from the scanner's hardware, e.g.,  $B_0$  drift, seem to have a minimal effect on the temporal stability of the FF measurements.

The validity of the co-registration method revealed a high registration accuracy of the *in vivo* data, indicated by the absence of any temporal pattern of the registration error and small FF changes over time. Due to the location of BAT in the supraclavicular area, the measurements are especially prone to movement artifacts. Indeed, our data show that co-registration reduces the within-subject variability two-fold compared to non-registered data while using mutual FF thresholding. This translated, on average, to double the scBAT FF reduction during cooling for non-registered data compared to registered data.

For non-registered data, mutual FF thresholding increased the within-subject variability by 23% compared to single FF thresholding. This increase is the result of large spatial mismatches between the reference scan and non-registered dynamics, which reduces the number of co-located voxels with a FF above 30% in both the reference scan and dynamic, thereby confirming the presence of motion across the dynamics. For registered data, mutual FF thresholding reduced the within-subject variability by 30% compared to single FF thresholded data. Since the spatial mismatches between the reference scan and registered dynamics are mostly resolved, the mutual thresholding approach only accounts for small spatial mismatches between scans that are still present after the registration, such as partial volume effects.

The added value of the co-registration is less pronounced when comparing registered- and non-registered data obtained with single FF thresholding, where the within-subject

variability was reduced by 23%. Nevertheless, by combining image registration and mutual FF thresholding, the within-subject variability of scBAT  $\Delta$ FF (MSE: 0.07% $\pm$ 0.05%) was further reduced by almost 2-fold compared to non-registered data obtained with single FF thresholding (MSE:0.13 $\pm$ 0.13%) and mutual FF thresholding (MSE: 0.16 $\pm$ 0.14). Our results, therefore highlight the importance of using both methods for these kind of tissues types that are prone to motion artefacts.

Compared to the literature where scans were obtained during cooling, our scBAT FF changes are generally smaller than those reported previously (-1.9%<sup>20</sup>, -2.9%<sup>15</sup>, -3.0%<sup>14,18</sup>, -3.5%<sup>24</sup>, -4.7%<sup>19</sup>). This could be due to several reasons, including the lack of breath-holds and/or co-registration or differences in previous study protocols. As a result, the reported scBAT FF changes may have been overestimated as a result of motion. Several studies did use co-registration in their analysis<sup>13,19,20</sup>, but images were acquired during free breathing. Since the registration error increases with the amount of image displacement<sup>24</sup>, it cannot be excluded that this may have influenced the outcomes. A previous study by Stahl et al used both image registration and breath-holds in their protocol<sup>15</sup>, but images were acquired using a two-echo Dixon protocol. It has been shown that a two-echo sequence overestimates the FF below 60% and underestimates the FF above 60% compared to a six-echo protocol<sup>25</sup>, which is the result of field inhomogeneities that are not corrected, and may therefore produce misleading scBAT  $\Delta$ FF outcomes.

Moreover, differences in the applied cooling procedures (e.g., cooling garments, duration, intensity, medium (i.e., water or air) or strategy (i.e., personalized or standardized) may also have contributed to the inconsistency in FF outcomes in the literature. Although participants reported an increased cold perception during cooling, a larger  $\Delta$ FF scBAT response may have occurred in previous studies<sup>18,19,24</sup> since participants were exposed to lower temperatures compared to our standardized mild-cooling protocol (18°C). Since no thermal perception scores were reported in these previous studies, this hypothesis should be further tested by comparing thermal perception measurements and scBAT  $\Delta$ FF outcomes across different cooling procedures.

Overall, scBAT FF changes were found to be significantly reduced with respect to the control tissues during the last 30 minutes of cooling. This gradual decrease in scBAT FF is most likely attributable to the combustion of lipids within the scBAT depot. While an increase in perfusion could produce a change in image intensity leading to an apparent reduction in scBAT FF, this seems unlikely for several reasons. First of all, Blondin et al. showed that BAT perfusion determined by <sup>11</sup>C-acetate PET-CT was unaltered after 3 hours of cold exposure in healthy adults, and that intracellular triglycerides were the primary fuel for BAT thermogenesis<sup>1</sup>. Secondly, Coolbaugh et al. reported a mean FF decrease of 14% in voxels with a FF in the 90-100% decile after 1-hour of personalized cold exposure<sup>16</sup>. The

authors argued that if half of the water signal came from blood at thermoneutrality (e.g., assuming a blood volume fraction of 2.5% at baseline), then the blood volume fraction would have increased by 16.5% to explain this reduction of 14%, which is very unlikely. In addition, Lundstrom et al., showed that the reduction in scBAT FF determined by MRI persisted after the cooling was removed, which argues against perfusion being a dominant factor since it would then be expected that the perfusion would decrease<sup>17</sup>. Finally, the gradual FF increase (+0.4% FF) at the onset of cooling is not in line with a major role of perfusion, as increased perfusion would be accompanied by an apparent immediate decrease scBAT FF due to the increased volume fraction of water.

To the best of our knowledge, this increase in FF upon cooling has not been reported before, but could be due to lipid uptake in scBAT from the blood prior to combustion. This would be in line with recent data from Straat et al., who showed that plasma triglyceride (TG) levels transiently decreased in response to cold exposure<sup>26</sup>. We postulate that soon after the initiation of cold exposure, BAT rapidly increases the uptake of triglyceride-derived fatty acids, resulting in the observed initial scBAT FF increase. Then, after eight minutes, the combustion of intracellular lipids possibly exceeds the uptake of fatty acids, leading to an overall decrease in scBAT FF. Future research could, therefore, combine these measures with repeated blood sampling to experimentally address this hypothesis.

This study has several limitations: in our protocol, 140 breath-holds of 16s were needed from the subject, which involved a high burden for patients. Since our data showed an inter-image variability (MSE) of less than 0.1% in scBAT, this may allow the use of lower time resolutions at intervals for which scBAT FF changes are stable (e.g., thermoneutrality or prolonged cooling<sup>14</sup>). Another limitation is that the study population only included young and healthy adults, and thus our results cannot be extrapolated to more general populations.

In conclusion, our MRI protocol and analysis pipeline enables 1-minute resolution measurements of scBAT  $\Delta$ FF with a small inter-image variability. Co-registration and mutual FF thresholding showed a two-fold lower variability compared to non-registered data, and its use is therefore highly recommended to improve the stability of scBAT  $\Delta$ FF measurements.

## REFERENCES

1. Blondin DP, Frisch F, Phoenix S, et al. Inhibition of Intracellular Triglyceride Lipolysis Suppresses Cold-Induced Brown Adipose Tissue Metabolism and Increases Shivering in Humans. *Cell Metabolism*. 2017;25(2):438-447. doi:10.1016/j.cmet.2016.12.005
2. Bartelt A, Bruns OT, Reimer R, et al. Brown adipose tissue activity controls triglyceride clearance. *Nature Medicine*. 2011;17(2):200-206. doi:10.1038/nm.2297
3. Oikonomou EK, Antoniades C. The role of adipose tissue in cardiovascular health and disease. *Nature Reviews Cardiology*. 2019;16(2):83-99. doi:10.1038/s41569-018-0097-6
4. Becher T, Palanisamy S, Kramer DJ, et al. Brown adipose tissue is associated with cardiometabolic health. *Nature Medicine*. 2021;27(1):58-65. doi:10.1038/s41591-020-1126-7
5. Van Der Lans AAJJ, Hoeks J, Brans B, et al. Cold acclimation recruits human brown fat and increases nonshivering thermogenesis. *Journal of Clinical Investigation*. 2013;123(8):3395-3403. doi:10.1172/JCI68993
6. Yoneshiro T, Aita S, Matsushita M, et al. Recruited brown adipose tissue as an antiobesity agent in humans. *The Journal of Clinical Investigation*. 2013;123(8):3404-3408. doi:10.1172/JCI67803
7. Cannon B, Nedergaard J. Brown Adipose Tissue: Function and Physiological Significance. *Physiological Reviews*. 2004;84(1):277-359. doi:https://doi.org/10.1152/physrev.00015.2003
8. Cypess AM, Weiner LS, Roberts-Toler C, et al. Activation of human brown adipose tissue by a  $\beta$ 3-adrenergic receptor agonist. *Cell metabolism*. 2015;21(1):33-38. doi:10.1016/J.CMET.2014.12.009
9. Chen KY, Cypess AM, Laughlin MR, et al. Brown Adipose Reporting Criteria in Imaging Studies (BARCIST 1.0): Recommendations for Standardized FDG-PET/CT Experiments in Humans. *Cell Metabolism*. 2016;24(2):210-222. doi:10.1016/j.cmet.2016.07.014
10. Schilperoort M, Hoeke G, Kooijman S, Rensen PCN. Relevance of lipid metabolism for brown fat visualization and quantification. *Current Opinion in Lipidology*. 2016;27(3):242-248. doi:10.1097/MOL.0000000000000296
11. Karampinos DC, Weidlich D, Wu M, Hu HH, Franz D. Techniques and Applications of Magnetic Resonance Imaging for Studying Brown Adipose Tissue Morphometry and Function. *Handbook of experimental pharmacology*. 2019;251:299-324. doi:10.1007/164\_2018\_158
12. Wu M, Junker D, Branca RT, Karampinos DC. Magnetic Resonance Imaging Techniques for Brown Adipose Tissue Detection. *Frontiers in Endocrinology*. 2020;11:421. doi:10.3389/FENDO.2020.00421/FULL
13. Gashi G, Madoer P, Maushart CI, et al. MRI characteristics of supraclavicular brown adipose tissue in relation to cold-induced thermogenesis in healthy human adults. *Journal of Magnetic Resonance Imaging*. 2019;50(4):1160-1168. doi:10.1002/jmri.26733
14. Oreskovich S, Ong F, Ahmed B, et al. Magnetic resonance imaging reveals human brown adipose tissue is rapidly activated in response to cold. *Journal of the Endocrine Society*. Published online October 14, 2019. doi:10.1210/js.2019-00309
15. Stahl V, Maier F, Freitag MT, et al. In vivo assessment of cold stimulation effects on the fat fraction of brown adipose tissue using DIXON MRI. *Journal of Magnetic Resonance Imaging*. 2017;45(2):369-380. doi:10.1002/jmri.25364
16. Reber J, Willershäuser M, Karlas A, et al. Non-invasive Measurement of Brown Fat Metabolism Based on Optoacoustic Imaging of Hemoglobin Gradients. *Cell metabolism*. 2018;27(3):689-701.e4. doi:10.1016/j.cmet.2018.02.002

17. Deng J, Neff LM, Rubert NC, et al. MRI characterization of brown adipose tissue under thermal challenges in normal weight, overweight, and obese young men. *Journal of magnetic resonance imaging : JMRI*. 2018;47(4):936-947. doi:10.1002/jmri.25836
18. Holstila M, Pesola M, Saari T, et al. MR signal-fat-fraction analysis and T2\* weighted imaging measure BAT reliably on humans without cold exposure. *Metabolism: Clinical and Experimental*. 2017;70:23-30. doi:10.1016/j.metabol.2017.02.001
19. Coolbaugh CL, Damon BM, Bush EC, Welch EB, Towse TF. Cold exposure induces dynamic, heterogeneous alterations in human brown adipose tissue lipid content. *Scientific Reports*. 2019;9(1):13600. doi:10.1038/s41598-019-49936-x
20. Lundström E, Strand R, Johansson L, Bergsten P, Ahlström H, Kullberg J. Magnetic resonance imaging cooling-reheating protocol indicates decreased fat fraction via lipid consumption in suspected brown adipose tissue. *PLoS ONE*. 2015;10(4). doi:10.1371/journal.pone.0126705
21. Hu HH, Yokoo T, Bashir MR, et al. Linearity and bias of proton density fat fraction as a quantitative imaging biomarker: A multicenter, multiplatform, multivendor phantom study. *Radiology*. 2021;298(3):640-651. doi:10.1148/RADIOL.2021202912/ASSET/IMAGES/LARGE/RADIOL.2021202912.TBL6.JPEG
22. Wang X, Hernando D, Reeder SB. Sensitivity of Chemical Shift-Encoded Fat Quantification to Calibration of Fat MR Spectrum. *Magnetic resonance in medicine*. 2016;75(2):845. doi:10.1002/MRM.25681
23. Abreu-Vieira G, Sardjoe Mishre A.S.D, Burakiewicz J, janssen L.G.M, Nahoj K.J, van der Eijk J.A, Riem T.T, Boon M.R, Dzyubachyk O, Webb A.G, Rensen P.C.N KHE. Human brown adipose tissue estimated with magnetic resonance imaging undergoes changes in composition after cold exposure: an in vivo MRI study in healthy volunteers. *Frontiers in Endocrinology*.
24. Kadoya N, Fujita Y, Katsuta Y, et al. Evaluation of various deformable image registration algorithms for thoracic images. *Journal of radiation research*. 2014;55(1):175-182. doi:10.1093/JRR/RRT093
25. Abreu-Vieira G, Sardjoe Mishre ASD, Burakiewicz J, et al. Human Brown Adipose Tissue Estimated With Magnetic Resonance Imaging Undergoes Changes in Composition After Cold Exposure: An in vivo MRI Study in Healthy Volunteers. *Frontiers in Endocrinology*. 2020;10. doi:10.3389/fendo.2019.00898
26. Cold Exposure Induces Dynamic Changes in Circulating Triacylglycerol Species, Which is Dependent on Intracellular Lipolysis: A Randomized Cross-Over by Maaïke Straat, Lucas Jurado Fasoli, Zhixiong Ying, Kimberly Nahon, Laura Janssen, Mariëtte Boon, Gernot Grabner, Sander Kooijman, Robert Zimmermann, Martin Giera, Patrick C.N. Rensen, Borja Martinez :: SSRN. Accessed July 20, 2022. [https://papers.ssrn.com/sol3/papers.cfm?abstract\\_id=4163695](https://papers.ssrn.com/sol3/papers.cfm?abstract_id=4163695)